Antiferroelectric lattice distortion induced by ferroquadrupolar order in $DyVO_4$

K. Kishimoto, T. Ishikura, H. Nakamura, Y. Wakabayashi, and T. Kimura
Division of Materials Physics, Graduate School of Engineering Science, Osaka University, Toyonaka, Osaka 560-8531, Japan
(Received 8 July 2010; published 27 July 2010)

The effects of quadrupolar order on structural, magnetic, and dielectric properties have been investigated for $DyVO_4$. Our detailed structure analysis demonstrated that the cooperative Jahn-Teller effect associated with $4f$ ferroquadrupolar order causes the displacement of oxygen ions surrounding a Dy ion, which makes the relative position of a V ion off-center in a VO_4 tetrahedron. The lattice distortion well explains antiferroelectriclike anomalies at around the quadrupolar ordering temperature. We also report the Jahn-Teller domain control giving rise to a remarkable magnetocapacitance effect by applying a small magnetic field (~0.1 T).

DOI: 10.1103/PhysRevB.82.012103 PACS number(s): 77.22.−d, 75.25.Dk, 71.70.Ej, 75.85.+t

There has been an upsurge of interest in magneto(di)electric phenomena in localized electron systems involving multiferroics in which magnetic and ferroelectric orders coexist and couple with each other.[1] The nomenclature "multiferroics" was originally coined for materials in which two or all three ferroic orders (ferroelectric, ferromagnetic, and ferroelastic) coexist in the same phase.[2,3] Besides these three orders, the ordering of quadrupole moments in d and f electron systems has also received much attention for many years.[4,5] When the quadrupolar interaction couples with the crystal lattice, the cooperative Jahn-Teller (JT) effect arises. Typical examples showing the JT effect induced by the quadrupolar interaction are rare-earth zircons such as $TbVO_4$ and $DyVO_4$ [Fig. 1(a)]. These rare-earth zircons undergo the JT transition from the $I4_1/amd$ tetragonal to an orthorhombic structure at T_D, which is associated with the ordering of $4f$ quadrupole moments of the rare-earth ions. There have been extensive studies on the spontaneous structural phase transition of the JT nature (quadrupolar ordering) in these rare-earth zircons for more than four decades.[6–15]

In $DyVO_4$, the ground state of the Dy^{3+} ($4f^9$, $^6H_{15/2}$) ion is a near accidental quartet consisting of two Kramers doublets ($|J=\frac{15}{2}, J_x=\pm J\rangle$ and $|J=\frac{15}{2}, J_y=\pm J\rangle$) above $T_D=14$ K while these doublets are split by the JT distortion below T_D.[4,7] The pairs of states $|\pm J_x\rangle$ and $|\pm J_y\rangle$ have $4f$ electron clouds in the shape of flat pancakes and correspond to electric quadrupoles. Thus, the quadrupolar order parameter is proportional to the expectation value of the quadrupole operator $Q_2=\alpha_J\langle O_2\rangle$, where α_J is the Stevens parameter and $O_2=J_x^2-J_y^2$. A ferroquadrupolar order, as illustrated in Fig. 1(b), appears below T_D and causes the lattice distortion along the [100] direction (B_{1g} strain, γ-symmetry distortion).[16,17] The lower-lying doublet is magnetically highly anisotropic and Ising type in character, which makes the JT transition controllable by magnetic fields. It is also known that the electric susceptibility χ shows remarkable anomalies accompanied by the ferroquadrupolar order.[11,12] The in-plane electric susceptibilities χ_a and χ_b show little temperature dependence above T_D but change substantially below T_D, and the difference between χ_a and χ_b was believed to be proportional to the order parameter. On the other hand, χ along the c axis (χ_c) exhibits Curie-type behavior above T_D and a prominent cusp at T_D, which is reminiscent of an (anti)ferroelectric transition. To explain the temperature dependence of χ_c, Unoki and Sakudo proposed the antiferroelectricity driven by the soft B_{1g} strain mode related to the ferroquadrupolar order.[12]

Unlike the case of $TbVO_4$, the mean-field approximation cannot describe the quadrupolar effects in $DyVO_4$ in which strong short-range interactions arise through the coupling of the Dy electronic levels to optical-phonon modes.[7,8] Therefore, a correlated effective field (CEF) theory considering the short-range interactions has been applied to explain the effects of the quadrupolar order on magnetic and dielectric properties in $DyVO_4$.[10,11] The order parameter of quadrupolar interaction is indispensable for the analysis. However, most of the previous studies derived the order parameter from the assumption that the in-plane anisotropy of χ, $\chi_a-\chi_b$, or that of the birefringence was proportional to the order parameter. To date, there have been few systematic experimental studies which directly observed the order parameter.[13] To verify the validity of the previous discussions, we investigated the crystal structure of $DyVO_4$ in detail by means of in-field synchrotron x-ray diffraction measurements and obtained the order parameter of quadrupolar interaction in various temperature (T) and magnetic field (B) conditions. The obtained order parameter was used to analyze the magnetization and the electric susceptibility in the framework of the CEF theory. Furthermore, we report on the complete crystal structure of the low-T orthorhombic phase and present direct evidence of antiferroelectric lattice distortion induced by the ferroquadrupolar order in $DyVO_4$.

We grew transparent yellowish single crystals of $DyVO_4$ by the floating-zone method, following Ref. 18. X-ray diffraction (XRD) measurements of the obtained single crystals were performed at the beamlines BL-3A and 8B of the Photon Factory, KEK. For the crystal structure analysis, oscillation images using an 18 keV x-ray were captured by an imaging plate (IP) Weissenberg camera. The crystal was cooled by a closed-cycle He refrigerator in which a permanent magnet was placed near the crystal to remove orthorhombic twin domains below T_D by applying a small B (~0.09 T). For the image data processing of digital IP data and structure refinement, the programs RAPID (Rigaku) and SHELX (Ref. 19) were used. Additionally, to investigate the effect of B on the order parameter and the domain rearrangement, in-field XRD measurements using a 14 keV x-ray were performed in an 8 T superconducting magnet. For these measurements, the crystal was oriented with the $[100]_{tetra}$ and the $[001]_{tetra}$ axes

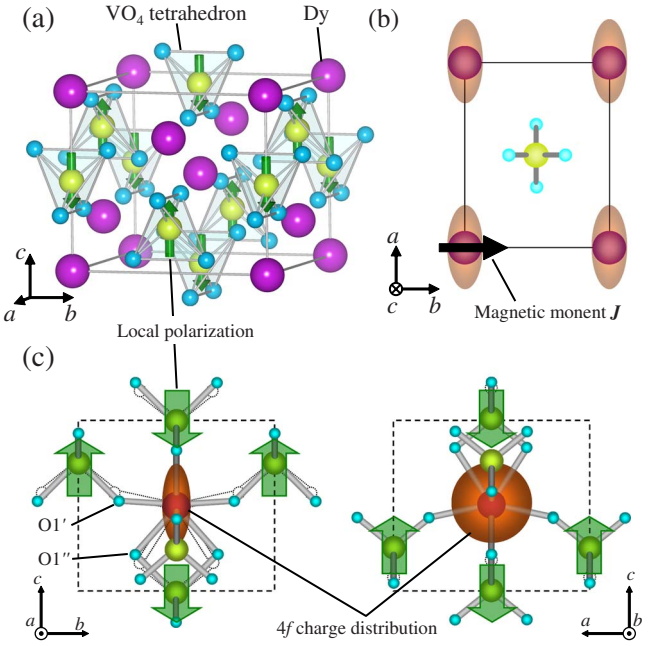

FIG. 1. (Color online) Crystal structure of $DyVO_4$. (a) Unit cell. (b) The projection along the c axis of the quadrupolar-ordered crystal structure below T_D. (c) The JT distortion in a unit cell. Dashed lines represent crystal structure in the high-T phase. Ellipses surrounding Dy ions in (b) and (c) indicate the schematic views of pancakelike charge distributions of 4f electrons. Thick arrows in (a) and (c) denote the direction of the local electric polarization in the respective VO_4 tetrahedra.

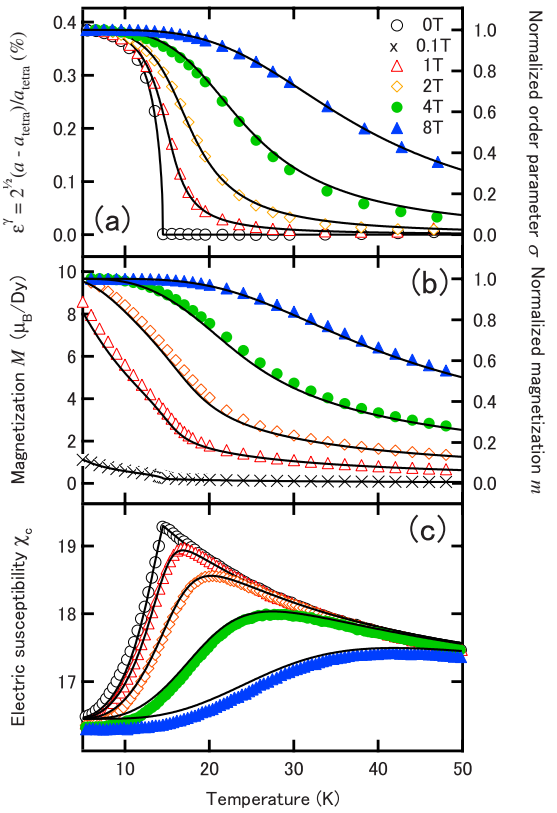

FIG. 2. (Color online) Temperature variations in (a) order parameter, (b) magnetization, and (c) electric susceptibility along the c axis at several magnetic fields for single crystals of $DyVO_4$. Magnetic fields were applied along $[100]_{tetra}$. Solid curves show the best least-squares fit of CEF theory to the experimental data points.

in the scattering plane, and B was applied parallel to $[010]_{tetra}$, where the suffix *tetra* denotes the tetragonal notation. Oscillation photographs around $(800)_{tetra}$, and thereby (800) and (080) in the orthorhombic phase, were integrated into 2θ profiles to obtain the lattice parameters a and b. The order parameter defined as the B_{1g} orthorhombic distortion, $\varepsilon^{\gamma}=\sqrt{2}(a-a_{tetra})/a_{tetra}$, was determined from the measured values of the lattice constant a. The magnetization, the electric susceptibility at 1 kHz, and the electric displacement at 375 kV/m were measured in superconducting magnets by using a commercial magnetometer, an *LCR* meter, and an electrometer, respectively. For all the in-field measurements, B was applied along the $[010]_{tetra}$ direction.

Figure 2 shows T variations in (a) the order parameter ε^{γ}, (b) the magnetization M, and (c) the electric susceptibility along the c axis χ_c at several magnetic fields. First, we focus on the experimental data in the absence of B. A finite ε^{γ} appears below $T_D=14$ K, which is attributed to the JT transition, i.e., the ferroquadrupolar ordering. Accompanied by this transition, M and χ_c also show anomalies. The onset of the transition was observed as a weak enhancement of M and a sharp cusp in χ_c at T_D. Another characteristic in χ_c is (anti)ferroelectriclike behaviors including a Curie-type T dependence above T_D and a sudden drop below T_D, which is consistent with the results reported previously.[11,12] The application of B makes ε^{γ} finite even above T_D and stabilizes the low-T phase. With increasing B, ε^{γ} increases above T_D while it remains constant at temperatures well below T_D. This is because the Zeeman splitting induced by the application of B promotes the alignment of J and the associated quadrupolar ordering. Above T_D, M (χ_c) drastically increases (decreases) in accordance with the enhancement of the order parameter by applied B.

To describe the observed T and B variations in ε^{γ}, M, and χ_c, we employed the CEF theory of the Ising model.[10,11] In the CEF theory, the T dependence of the normalized order parameter σ and the correlation parameter α is obtained from the self-consistent solutions of the equations,

$$\sigma = \tanh[\beta J'(1-\alpha)\sigma], \tag{1}$$

$$\alpha = \langle \varphi_q/[1-\beta J'(1-\sigma^2)(\varphi_q-\alpha)]\rangle_q, \tag{2}$$

where J' is the total JT coupling and $\langle\cdots\rangle_q$ denotes $N^{-1}\Sigma_q(\cdots)$. Following the analysis described in Ref. 11, we also used the parametrized form of φ_q given in Ref. 10. In the presence of B along b (or a) which causes the Zeeman splitting, the normalized order parameter σ and the normalized magnetization m can be written as

$$\sigma = 1 - 2/\{\exp[2\beta J'(1-\alpha)\sigma]\cosh(\beta H_M) + 1\}, \tag{3}$$

TABLE I. Structural parameters of $DyVO_4$ at 20 and 13 K. Atomic positions for the $I4_1/amd$ symmetry are, for Dy, $4b(\frac{1}{2},\frac{1}{4},\frac{1}{8})$, V, $4a(\frac{1}{2},\frac{1}{4},-\frac{3}{8})$, and O1, $16h(x,\frac{1}{4},z)$; and for *Imma* symmetry Dy, $4e(0,\frac{1}{4},z)$, V, $4e(\frac{1}{2},\frac{1}{4},\frac{1}{8})$, O1, $8i(x,\frac{1}{4},z)$, and O2, $8h(0,y,z)$. The positions of O1′ and O1″ are shown in Fig. 1(c).

T	20 K	13 K
Space group	$I4_1/amd$	*Imma*
a (Å)	7.1343(16)	7.1479(13)
b (Å)		7.1247(16)
c (Å)	6.2950(15)	6.2956(11)
$R1$ (%)	2.60	2.21
Dy z		0.87479(4)
O1 x	0.3160(4)	−0.1846(3)
O1 z	−0.5450(2)	0.5466(3)
O2 y		0.4346(6)
O2 z		0.1987(3)
Dy-O1′ (Å)	2.310(3)	2.294(4)
Dy-O1″ (Å)	2.458(2)	2.427(3)
O1′-Dy-O1″ (deg)	70.31(6)	68.80(9)

$$m = \frac{1}{2}(1+\sigma)\tanh(\beta H_M). \tag{4}$$

Here $H_M = \frac{1}{2}g\mu_B(B+B_d m)$ in which B_d is the correction field for the demagnetization effect. These equations can be solved self-consistently, and the equilibrium values of σ, α, and m can be obtained as functions of T and B. Additionally, χ_c can be written as

$$\chi_c = \chi_0[1-(J'_u-\mu_u)g_r^{zz}]/(1-J'_u g_r^{zz}), \tag{5}$$

$$g_r^{zz} = \beta(1-\sigma^2)/[1+\alpha J'\beta(1-\sigma^2)], \tag{6}$$

where χ_0, J'_u, and μ_u are treated as fitting parameters. To compare our experimental results with those of the CEF theory, we first obtained σ as functions of T and B by fitting the experimental results of ε^γ at various T and B. Next, using the obtained σ, we fit the experimentally obtained M and χ_c from Eqs. (4) and (5), respectively. Solid lines in Fig. 2 show the best least-squares fit of the CEF theory and reproduce the experimental results well. The results confirm that dielectric and magnetic properties can be completely described by the order parameter in this system.

The fundamental crystal structure of $DyVO_4$ is composed of alternating VO_4 tetrahedra and DyO_8 triangulated dodecahedra connected over common edges, as illustrated in Fig. 1(a). Table I gives lists of the final refined parameters obtained from the crystal structure analysis for the data at 20 and 13 K. The obtained space groups, $I4_1/amd$ above T_D and *Imma* below T_D, are consistent with the previously reported symmetry. In the $I4_1/amd$ tetragonal phase, a Dy ion has four nearest-neighbor O ions and the four Dy-O bond lengths are equivalent. In addition, all four V-O bond lengths in a VO_4 tetrahedron are also equivalent and the V ion is seated

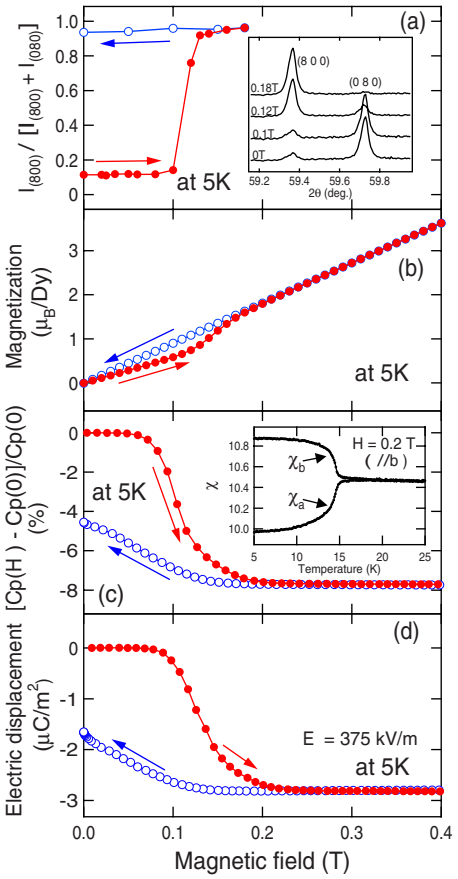

FIG. 3. (Color online) Magnetic field dependence of (a) relative intensity of the (800) peak, (b) magnetization, (c) magnetocapacitance, and (d) electric displacement measured in an applied electric field at 5 K for single crystals of $DyVO_4$. Magnetic fields were applied along $[100]_{tetra}$. Inset of (a): the (800)/(080) Bragg reflection profiles at selected B in the increasing B run. Inset of (c): T profiles of χ_a and χ_b at 0.2 T.

at the center of gravity in the tetrahedron. These configurations change in the *Imma* orthorhombic phase in which there are two nonequivalent oxygen sites.

We plot in Fig. 1(c) the detailed deformations of alternating VO_4 tetrahedra and DyO_8 dodecahedra in the *Imma* orthorhombic phase. Both Dy-O1′ and Dy-O1″ bonds lying in the bc plane shorten, and the O1′-Dy-O1″ bond angle becomes smaller below T_D. It is natural to consider that the observed deformation of the DyO_8 dodecahedra arises from the ferro-ordering of a pancake-shaped quadrupole which is illustrated as an orange ellipse (circle) in the left (right) panel of Fig. 1(c). Since the DyO_8 dodecahedra are connected with the VO_4 tetrahedra over common edges, the deformation of the DyO_8 dodecahedra also causes that of the VO_4 tetrahedra, as illustrated in Fig. 1(c). As a consequence, the gravity of the four oxygen ions in a VO_4 tetrahedron shifts slightly along the c axis, and then the relative position of the V ion is off-centered in the tetrahedron, which creates a local polarization along the c axis. The directions of the local polarization in the respective VO_4 tetrahedra align alternately between adjacent tetrahedra, as denoted by thick arrows in Figs. 1(a) and 1(c). Thus, the low-T structure obtained here

demonstrates that the ferroquadrupolar order on Dy sites drives the antiferroelectric lattice distortion related to the deformation of VO_4 tetrahedra and well explains the antiferroelectriclike behavior in χ_c.

Finally, we present the structural domain control giving rise to a remarkable magnetocapacitance effect by applying a relatively small B ($\sim$0.1 T) below T_D. Orthorhombic twin domains develop below T_D and can be detected by a splitting between the (800) and the (080) Bragg peaks, as shown in the inset of Fig. 3(a). At 0 T, both peaks are present. When B is applied, the intensity of the (800) and the (080) peaks suddenly increases and decreases at around 0.1 T, respectively. Above $\sim$0.15 T, the (080) peak completely vanishes while the intensity of the (080) peak is saturated, which means the crystal becomes a single domain. Once the crystal is detwinned, it remains a single domain even after the removal of B [blue open circles in Fig. 3(a)]. This result confirms that B applied along one of the distortion directions produced a single domain crystal, and the crystallographic distortion can be switched to the other possible direction. The structural switching, that is, the rearrangement of quadrupole, is triggered by a B-induced 90° rotation of J, which can be observed as a sudden jump of M [Fig. 3(b)].

We observed a remarkable magnetocapacitance effect accompanied by the switching. As shown in Fig. 3(c), the application of B induces a fairly large suppression of the sample capacitance C at around 0.1 T. Before this measurement, we first made the sample a single domain by applying B and then removed B. Subsequently, we measured C along the a axis as a function of B applied along the b axis. The change in C is ascribed to two contributions: the change in capacitor dimensions, i.e., the difference between a and b, and the change in the sample permittivity, i.e., the difference between χ_a and χ_b. The former and the latter contributions account for about 10% and 90% of the observed change in C.[11] For reference, we show in the inset of Fig. 3(c) T profiles of χ_a and χ_b which are obtained by considering the T dependence of a and b. The B-induced change in C naturally causes that of electric displacement D. Figure 3(d) shows the B dependence of D measured at an applied electric field E of 375 kV/m. In accordance with the structural switching at $\sim$0.1 T, a sudden change in D is observed. This remarkable change in D observed at the domain switching in $DyVO_4$ resembles the magnetoelectric effect in multiferroics, though the application of E is needed for the present observation.

In summary, we examined the effects of the ordering of quadrupole moments (Jahn-Teller transition) on structural, magnetic, and dielectric properties in a $4f$ electron system, $DyVO_4$. Our experimental results are well explained by the analysis based on the correlated effective theory. Furthermore, we demonstrate an antiferroelectric lattice distortion induced by the ferroquadrupolar order and magnetically controllable dielectric properties through the magnetic control of the Jahn-Teller order parameter and domain structure.

We would like to thank A. P. Ramirez for stimulating discussions. This work was supported by KAKENHI (Grants No. 20674005 and No. 20001004) and Global COE Program (G10), MEXT, Japan.

[1] W. Eerenstein, N. D. Mathur, and J. F. Scott, Nature (London) **442**, 759 (2006).
[2] H. Schmid, Ferroelectrics **62**, 317 (1994).
[3] N. A. Hill, J. Phys. Chem. B **104**, 6694 (2000).
[4] G. A. Gehring and K. A. Gehring, Rep. Prog. Phys. **38**, 1 (1975).
[5] Y. Tokura and N. Nagaosa, Science **288**, 462 (2000).
[6] A. H. Cooke, C. J. Ellis, K. A. Gehring, M. J. M. Leask, D. M. Martin, B. M. Wanklyn, M. R. Wells, and R. L. White, Solid State Commun. **8**, 689 (1970).
[7] R. J. Elliott, R. T. Harley, W. Hayes, and S. R. P. Smith, Proc. R. Soc. London, Ser. A **328**, 217 (1972).
[8] J. R. Sandercock, S. B. Palmer, R. J. Elliott, W. Hayes, S. R. Smith, and A. P. Young, J. Phys. C **5**, 3126 (1972).
[9] B. G. Vekhter and M. D. Kaplan, Fiz. Tverd. Tela (Leningrad) **20**, 1433 (1978).
[10] S. R. P. Smith, J. Phys. C **17**, 41 (1984).
[11] J. H. Page, D. R. Taylor, and S. R. Smith, J. Phys. C **17**, 51 (1984).
[12] H. Unoki and T. Sakudo, Phys. Rev. Lett. **38**, 137 (1977).
[13] Z. A. Kazeĭ, N. P. Kolmakova, I. B. Krynetskiĭ, A. A. Sidorenko, and L. V. Takunov, Phys. Solid State **42**, 285 (2000).
[14] S. J. Blundell, I. M. Marshall, W. Hayes, and F. L. Pratt, Phys. Rev. B **70**, 212408 (2004).
[15] C. Detlefs, F. Duc, Z. A. Kazeĭ, J. Vanacken, P. Frings, W. Bras, J. E. Lorenzo, P. C. Canfield, and G. L. J. A. Rikken, Phys. Rev. Lett. **100**, 056405 (2008).
[16] F. Sayetat, Solid State Commun. **10**, 879 (1972).
[17] H. Göbel and G. Will, Phys. Status Solidi B **50**, 147 (1972).
[18] K. Oka, H. Unoki, H. Shibata, and H. Eisaki, J. Cryst. Growth **286**, 288 (2006).
[19] G. M. Sheldrick, Acta Crystallogr., Sect. A: Found. Crystallogr. **64**, 112 (2008).